LARGE EDDY SIMULATION OF A TURBULENT NONPREMIXED JET FLAME USING A FINITE-RATE CHEMISTRY MODEL

by

Patrick H. Pisciuneri

B.E., Youngstown State University, 2006

Submitted to the Graduate Faculty of

the Swanson School of Engineering in partial fulfillment

of the requirements for the degree of

Master of Science

University of Pittsburgh

2008

UNIVERSITY OF PITTSBURGH

SWANSON SCHOOL OF ENGINEERING

This thesis was presented

by

Patrick H. Pisciuneri

It was defended on

November 12, 2008

and approved by

Dr. Peyman Givi, William K. Whiteford Professor of Mechanical Engineering and Materials Science

Dr. John A. Barnard, James T. MacLeod Professor of Mechanical Engineering and Materials Science

Dr. Bong Jae Lee, Assistant Professor of Mechanical Engineering and Materials Science

Thesis Advisor: Dr. Peyman Givi, William K. Whiteford Professor of Mechanical Engineering and Materials Science

LARGE EDDY SIMULATION OF A TURBULENT NONPREMIXED JET FLAME USING A FINITE-RATE CHEMISTRY MODEL

Patrick H. Pisciuneri, M.S.

University of Pittsburgh, 2008

Large eddy simulation (LES) is conducted of a turbulent piloted nonpremixed methane jet flame. This flame has been studied experimentally at Sandia National Laboratories.[1,2] The subgrid scale (SGS) closure in LES is based on the scalar filtered mass density function (SFMDF) methodology.[3] The SFMDF is essentially the mass weighted probability density function (PDF) of the SGS scalar quantities.[4] The SFMDF is obtained from an exact transport equation which provides a closed form for the chemical reaction effects. The unclosed terms in this equation are modeled by a set of stochastic differential equations (SDEs). The SDEs are solved by a hybrid finite-difference/Lagrangian Monte Carlo procedure. This flame exhibits little local extinction. In previous work,[5] the instantaneous flame composition was related to the mixture fraction based on the flamelet model at low strain rates. In the present work, this assumption is relaxed, and a direct solver is employed for finite-rate chemistry. The results via this method agree favorably with those obtained experimentally. The end result is an accurate and affordable method for the LES of realistic turbulent flames.

TABLE OF CONTENTS

LIST OF TABLES

LIST OF FIGURES

ACKNOWLEDGMENTS

I would like to thank my advisor, Dr. Peyman Givi, for his guidance throughout the course of my research, and for providing me with the opportunity to continue my graduate studies. I would also like to thank my colleagues at the Laboratory of Computational Transport Phenomena at the University of Pittsburgh, especially Dr. Reza Sheikhi, Server Levent Yilmaz, and Mehdi Bostandoost Nik who have all greatly contributed to my growth as a student and a researcher. I am grateful to the members of my thesis defense committee, Dr. John A. Barnard and Dr. Bong Jae Lee.

This work is part of research sponsored by the United States Air Force Office of Scientific Research (AFOSR) through Grant FA9550-06-1-0015 under the management of Dr. Julian M. Tishkoff, and the National Science Foundation (NSF) through Grant CTS-0426857. Computational resources are provided by the Pittsburgh Supercomputing Center (PSC), under TeraGrid Grant CTS070048.

1.0 INTRODUCTION

The filtered density function (FDF) methodology is becoming very popular for subgrid scale (SGS) modeling as required for large eddy simulation (LES) of turbulent reacting flows.[6,7] The FDF methodology was first introduced by Givi[8] and Pope,[9] and it serves as a counterpart to the probability density function (PDF) approach used in Reynolds averaged simulations (RAS).[9] The LES/FDF methodology is inherently suited for the treatment of large scale, unsteady phenomena. Thus, in comparison to RAS, it provides a more detailed and reliable prediction of turbulent reacting flows.

The FDF method has evolved considerably since its inception. The marginal scalar FDF (SFDF) provides the solution of the transported FDF, and it was first developed by Colucci *et al.*[10] for constant density flows. The variable density form of the SFDF was developed by Jaberi *et al.*,[3] and it is known as the scalar filtered mass density function (SFMDF). Gicquel *et al.*[11] developed the velocity FDF (VFDF) method in which the effects of SGS velocity convection appear in closed form. Joint velocity-scalar approaches was developed for constant density (VSFDF) and variable density (VSFMDF) flows by Sheikhi *et al.*[12,13]

In this work, the SFMDF is employed for the simulation of a piloted jet flame studied in the experiments of the Combustion Research Facility at the Sandia National Laboratories.[1,14] In these experiments, three turbulent flames were considered, labeled Flames D, E and F. The three flames are of the same geometrical configuration; however, the jet inlet velocity is varied for each flame. Sandia Flame D has the smallest jet inlet velocity, and it is such that the flame is close to equilibrium. Sandia Flames E and F have higher jet inlet velocities, such that noticeable non-equilibrium effects are present. Because Sandia Flame D is close to equilibrium, it is possible to determine all thermochemical variables from the mixture fraction,[15] as this has been demonstrated by Sheikhi *et al.*[5] However, due to the non-

equilibrium effects in Sandia Flames E and F, the near equilibrium assumption is not valid, and finite-rate chemistry models are required. The objective of this work is to simulate Sandia Flame D using a finite-rate chemistry model. The success of this work is necessary before we hope to successfully simulate Flames E and F.

2.0 FORMULATION

2.1 GOVERNING EQUATIONS

Implementation of LES involves the use of the spatial filtering operation,[4,16]

$$\langle f(\mathbf{x},t)\rangle_\ell = \int_{-\infty}^{+\infty} f(\mathbf{x}',t)\mathcal{G}(\mathbf{x}',\mathbf{x})\mathrm{d}\mathbf{x}' \tag{2.1}$$

where $\mathcal{G}$ denotes the filter function of width Δ_G, $\langle f(\mathbf{x},t)\rangle_\ell$ represents the filtered value of the transport variable, $f(\mathbf{x},t)$. In variable density flows it is convenient to consider the Favre filtered quantity $\langle f(\mathbf{x},t)\rangle_L = \langle \rho f\rangle_\ell / \langle\rho\rangle_\ell$. We consider spatially and temporally invariant and localized filter functions, $\mathcal{G}(\mathbf{x}',\mathbf{x}) \equiv G(\mathbf{x}'-\mathbf{x})$, with the properties $G(\mathbf{x}) = G(-\mathbf{x})$ and $\int_{-\infty}^{+\infty} G(\mathbf{x})\mathrm{d}\mathbf{x} = 1$.[17] Moreover, we only consider "positive" filter functions for which all the moments $\int_{-\infty}^{+\infty} x^m G(x)\mathrm{d}x$ exist for $m \geq 0$.[18]

Formulation is based on the compressible form of the continuity, Navier-Stokes, energy and species mass fraction conservation equations in a low Mach number flow. These equations govern the space ($\mathbf{x} \equiv x_i,\ i = 1,2,3$) and time ($t$) variations of the fluid density ($\rho(\mathbf{x},t)$), the velocity vector ($\mathbf{u} \equiv u_i(\mathbf{x},t)$), the specific enthalpy ($h(\mathbf{x},t)$), and the mass fractions of N_s species (Y_α ($\alpha = 1,2,\ldots,N_s$)). Further, we consider Fourier's law of heat conduction, Fick's law of diffusion, and we assume unity Lewis number. Applying the filtering operation to the conservation equations yields:

$$\frac{\partial\langle\rho\rangle_\ell}{\partial t} + \frac{\partial\langle\rho\rangle_\ell\langle u_i\rangle_L}{\partial x_i} = 0 \tag{2.2}$$

$$\frac{\partial\langle\rho\rangle_\ell\langle u_j\rangle_L}{\partial t} + \frac{\partial\langle\rho\rangle_\ell\langle u_i\rangle_L\langle u_j\rangle_L}{\partial x_i} = -\frac{\partial\langle p\rangle_\ell}{\partial x_j} + \frac{\partial\langle\tau_{ij}\rangle_\ell}{\partial x_i} - \frac{\partial T_{ij}}{\partial x_i} \tag{2.3}$$

$$\frac{\partial\langle\rho\rangle_\ell\langle\phi_\alpha\rangle_L}{\partial t} + \frac{\partial\langle\rho\rangle_\ell\langle u_i\rangle_L\langle\phi_\alpha\rangle_L}{\partial x_i} = -\frac{\partial\langle J_i^\alpha\rangle_\ell}{\partial x_i} - \frac{\partial M_i^\alpha}{\partial x_i} + \langle\rho\rangle_\ell\langle S_\alpha\rangle_L \tag{2.4}$$

where $\phi_\alpha \equiv Y_\alpha$ ($\alpha = 1, \ldots, N_s$), $\phi_\sigma \equiv h = \sum_{\alpha=1}^{N_s} h_\alpha Y_\alpha$, S_α is the production rate of species α, and $T_{ij} = \langle\rho\rangle_\ell(\langle u_i u_j\rangle_L - \langle u_i\rangle_L\langle u_j\rangle_L)$ and $M_i^\alpha = \langle\rho\rangle_\ell(\langle u_i\phi_\alpha\rangle_L - \langle u_i\rangle_L\langle\phi_\alpha\rangle_L)$ represent the subgrid stress and subgrid mass flux, respectively.

Equations 2.2, 2.3, 2.4 are closed by an equation of state,

$$\langle p\rangle_\ell = \langle\rho\rangle_\ell\langle\mathcal{R}T\rangle_L \tag{2.5}$$

where $\mathcal{R} = \mathcal{R}_0\sum_{\alpha=1}^{Ns} Y_\alpha/W_\alpha$, $\mathcal{R}_0$ is the universal gas constant, W_α is the molecular weight of species α, and T is the temperature. τ_{ij} and J_i^α denote the viscous stress tensor and the scalar fluxes, respectively:

$$\langle\tau_{ij}\rangle_\ell = \langle\mu\rangle_\ell\left(\frac{\partial\langle u_i\rangle_L}{\partial x_j} + \frac{\partial\langle u_j\rangle_L}{\partial x_i} - \frac{2}{3}\frac{\partial\langle u_k\rangle_L}{\partial x_k}\delta_{ij}\right) \tag{2.6}$$

$$\langle J_i^\alpha\rangle_\ell = -\gamma\frac{\partial\langle\phi_\alpha\rangle_L}{\partial x_i} \tag{2.7}$$

where μ is the molecular viscosity, which increases with temperature (T) to the power of 0.7, $\gamma = \langle\mu\rangle_\ell/Sc$ is the molecular diffusivity, and Sc is the molecular Schmidt number.

The closure problem of the SGS hydrodynamics is associated with the subgrid stress (T_{ij}) and subgrid mass flux (M_i^α). To model these terms, the modified kinetic energy viscosity (MKEV)[3] model is used. It is essentially a modified version of the gradient diffusion model proposed by Bardina *et al.*[19] The SGS stresses are modeled by,

$$T_{ij} = -2C_R\langle\rho\rangle_\ell\Delta_G\mathcal{E}^{1/2}\left(\langle\mathcal{S}_{ij}\rangle_L - \frac{1}{3}\langle\mathcal{S}_{kk}\rangle_L\delta_{ij}\right) + \frac{2}{3}C_I\langle\rho\rangle_\ell\mathcal{E}\delta_{ij} \tag{2.8}$$

where $\langle\mathcal{S}_{ij}\rangle_L$ is the resolved strain rate tensor and $\mathcal{E} = |\langle u_i^*\rangle_L\langle u_i^*\rangle_L - \langle\langle u_i^*\rangle_L\rangle_{\ell'}\langle\langle u_i^*\rangle_L\rangle_{\ell'}|$, with $u_i^* = u_i - \mathcal{U}_i$, where $\mathcal{U}_i$ is a reference velocity in the x_i direction. The subscript ℓ' denotes a filter at a secondary level of size $\Delta_{G'} > \Delta_G$. The subgrid eddy viscosity is expressed as $\nu_t = C_R\Delta_G\mathcal{E}^{1/2}$. The SGS mass fluxes are modeled by a similar model,[20]

$$M_i^\alpha = -\gamma_t\frac{\partial\langle\phi_\alpha\rangle_L}{\partial x_i} \tag{2.9}$$

where $\gamma_t = \langle\rho\rangle_\ell\nu_t/Sc_t$ is the subgrid diffusivity, and Sc_t is the subgrid Schmidt number.

2.2 SCALAR FILTERED MASS DENSITY FUNCTION

The SFMDF of the scalar array, $\boldsymbol{\phi}(\mathbf{x},t)$, is denoted by $\mathcal{F}_L(\boldsymbol{\psi};\mathbf{x},t)$ where $\boldsymbol{\psi}$ represents the composition domain of the scalar array. It is responsible for the SGS closure of the scalar array. A detailed derivation of the SFMDF transport equation was presented by Jaberi *et al.*;[3] therefore, only the final modeled transport equation will be presented here:

$$\frac{\partial \mathcal{F}_L}{\partial t}+\frac{\partial \langle u_i\rangle_L \mathcal{F}_L}{\partial x_i}=\frac{\partial}{\partial x_i}\left[(\gamma+\gamma_t)\frac{\partial \mathcal{F}_L/\langle\rho\rangle_\ell}{\partial x_i}\right]+\frac{\partial}{\partial \psi_\alpha}\left[\Omega_m\left(\psi_\alpha-\langle\phi_\alpha\rangle_L\right)\mathcal{F}_L\right]-\frac{\partial \hat{S}_\alpha \mathcal{F}_L}{\partial \psi_\alpha} \quad (2.10)$$

In Eq. 2.10, $\hat{S}_\alpha$ indicates that the production rate of species α can be completely described by the scalar array $\left(S_\alpha \equiv \hat{S}_\alpha\left(\boldsymbol{\phi}(\mathbf{x},t)\right)\right)$, and $\Omega_m = C_\Omega(\gamma+\gamma_t)/\left(\langle\rho\rangle_\ell \Delta_G^2\right)$ is the subgrid mixing frequency as required by the linear mean-square estimation (LMSE)[21,22] model for the closure of SGS mixing.

The SFMDF transport is alternatively represented by the general diffusion process governed by the SDE,[23,24]

$$\mathrm{d}X_i(t)=D_i\left(\mathbf{X}(t),t\right)\mathrm{d}t+E\left(\mathbf{X}(t),t\right)\mathrm{d}W_i(t) \quad (2.11)$$

where X_i denotes the Lagrangian position, D_i is the "drift" coefficent, E is the "diffusion" coefficient, and W_i denotes the Wiener process.[25] The SDEs used in this work are

$$\mathrm{d}x_i^+=\left[\langle u_i\rangle_L+\frac{1}{\langle\rho\rangle_\ell}\frac{\partial(\gamma+\gamma_t)}{\partial x_i}\right]\mathrm{d}t+\sqrt{\frac{2(\gamma+\gamma_t)}{\langle\rho\rangle_\ell}}\mathrm{d}W_i(t) \quad (2.12)$$

$$\mathrm{d}\phi_\alpha^+=\left[-\Omega_m\left(\phi_\alpha^+-\langle\phi_\alpha\rangle_L\right)+\hat{S}_\alpha\left(\boldsymbol{\phi}^+\right)\right]\mathrm{d}t \quad (2.13)$$

where x_i^+ and ϕ_α^+ denote the Lagrangian position and composition, respectively. The solution of these SDEs represents the solution of the SFMDF transport equation in the probablistic sense based on the principal of *equivalent systems*.[26,27]

2.3 CHEMISTRY MECHANISM

The chemical mechanism used in this work is the augmented reduced mechanism (ARM) of Sung *et al.*[28] It was derived from GRI-mech 1.2 for methane oxidation, and has been tested, in particular, for counterflow nonpremixed flames with extinction and ignition. This mechanism has been used extensively in PDF simulations of Sandia Flame D, and it generates results which are in good agreement with the experimental data.[29] It features 16 species and 12 reaction steps, which are presented in Table 1.

Table 1: ARM Reaction Steps and Species

Step	Reaction
1	$O_2 + 2CO = 2CO_2$
2	$H + O_2 + CO = OH + CO_2$
3	$H_2 + O_2 + CO = H + OH + CO_2$
4	$HO_2 + CO = OH + CO_2$
5	$O_2 + H_2O_2 + CO = OH + HO_2 + CO_2$
6	$O_2 + \frac{1}{2}C_2H_2 = H + CO_2$
7	$O_2 + CH_3 + CO + C_2H_4 = CH_4 + CO_2 + CH_2O + \frac{1}{2}C_2H_2$
8	$O_2 + 2CH_3 = H_2 + CH_4 + CO_2$
9	$O_2 + 2CH_3 + CO = CH_4 + CO_2 + CH_2O$
10	$O_2 + CH_3 + CO = H + CO_2 + CH_2O$
11	$O_2 + CO + C_2H_6 = CH_4 + CO_2 + CH_2O$
12	$H + OH = H_2O$

2.4 NUMERICAL SOLUTION PROCEDURE

Numerical solution of the equations governing the resolved field is based on a hybrid finite-difference/Monte Carlo method. In this method, the hydrodynamic variable equations are integrated by a finite-difference method, whereas the scalar field is simulated by the Monte Carlo method. More information about all the details and caveats of this solution procedure can be found in previous work.[3,10]

Calculation of the chemical source term proves to be computationally challenging. Methods, such as ISAT,[30] have been developed to efficiently calculate the chemical source term. However, the gains in efficiency introduce interpolation errors, and are only valid for the integration of the chemical source term, not the entire RHS of Eq. 2.13. Therefore, some type of splitting scheme must be used so that the effects of mixing and reaction can be treated separately. In an effort to avoid these issues, we opted for the direct integration of Eq. 2.13 by coupling a stiff ODE solver[31] with the CHEMKIN libraries.[32]

3.0 RESULTS

3.1 FLOW CONFIGURATION

Sandia Flame D consists of a main jet with a mixture of 25% methane (CH_4) and 75% air (21% O_2, 79% N_2) by volume in an ambient coflow of air. The main jet is stabilized by a pilot region consisting of a lean ($\Phi = 0.77$) mixture of acetylene (C_2H_2), hydrogen (H_2), air, carbon dioxide (CO_2) and nitrogen (N_2) with the same equilibrium composition as the main jet at a temperature of 1880 K. A schematic of the flame configuration is presented in Figure 1. The temperature of the jet is maintained at 294 K, and the coflow temperature measures 291 K. The Reynolds number of the jet is Re = 22400, with the jet diameter $D = 7.2$ mm and the bulk jet velocity equal to 49.6 m/s. Additional information about all the details of Sandia Flame D can be found on the Sandia web site.[2]

3.2 NUMERICAL SPECIFICATIONS

The simulation was conducted on a three-dimensional Cartesian mesh covering a domain of the size $16D \times 8D \times 8D$ in the x, y, and z directions respectively, mapped out over $81 \times 81 \times 81$ uniformly spaced finite-difference grid points, where D is the diameter of the jet. The filter size is set as $\Delta_G = 2\left(\Delta x \Delta y \Delta z\right)^{1/3}$, where Δx, Δy, and Δz denote the grid spacings in each of the corresponding directions. Other simulation parameters are presented in Table 2. The composition values at the inflow were set in accordance with the experimental values as reported by Xu and Pope,[29] and are also summarized in Table 3.

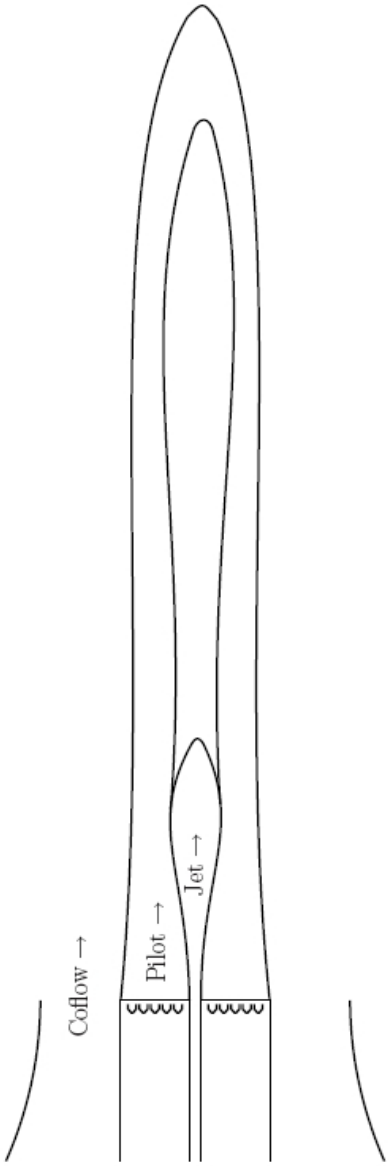

Figure 1: Sandia Flame D configuration.

Table 2: Simulations Parameters

Parameter	Description	Value
C_R	MKEV model parameter	0.02
C_I	MKEV model parameter	0.00
C_Ω	SGS mixing frequency	8.00
Sc	Schmidt number	0.75
Sc_t	SGS Schmidt number	0.75

3.3 COMPARISONS WITH EXPERIMENTAL DATA

The predictive capability of LES/SFMDF is demonstrated by comparing flow statistics with the available experimental data. These statistics are generated by long-time averaging of the instantaneous filtered flow variables for 2 residence times. For the purpose of flow visualization, instantaneous contour plots of some of the transport variables are presented in Figure 2. The figure shows that the growth of perturbations at the inflow is manifested downstream by the formation of large-scale coherent vortices. The upstream feedback from the vortices created initially triggers further self-sustaining vortex rollup, and subsequent pairing and coalescence of neighboring vortices.[33,34] The simulated data are statistically analyzed. For this purpose, a total of approximately 29,000 samples of several of the flow variables are collected during this recording period. In Figures 3 - 13 , $\overline{Q}$ and RMS(Q) denote, respectively, the time averaged mean and root mean square values of the variable Q.

The mean and RMS values of the axial velocity at the centerline are shown in Figure 3. The predicted results are in good agreement with the experimental data, indicating that the flow is adequately excited.

The radial distribution of the mean and RMS values of temperature and mixture fraction are shown in Figures 4 and 5 respectively. The means of each quantity are in good agreement

Table 3: Inlet Composition[a] Boundary Conditions

	Pilot	Coflow	Jet
T(K)	1880	291	294
P(atm)	.993	.993	.993
H_2	$1.7762E-03$	0.	0.
H	$6.9384E-04$	0.	0.
O_2	$4.7154E-02$	$2.1200E-01$	$1.5750E-01$
OH	$4.5794E-03$	0.	0.
H_2O	$1.4512E-01$	$1.0000E-02$	0.
HO_2	0.	0.	0.
H_2O_2	0.	0.	0.
CH_3	0.	0.	0.
CH_4	0.	0.	$2.5000E-01$
CO	$4.0243E-03$	0.	0.
CO_2	$6.9245E-02$	0.	0.
CH_2O	0.	0.	0.
C_2H_2	0.	0.	0.
C_2H_4	0.	0.	0.
C_2H_6	0.	0.	0.
N_2	$7.2740E-01$	$7.7800E-01$	$5.9250E-01$

[a] Species compositions are in mole fractions

with the experimental results, as well as the resolved RMS values. However, the total RMS values (resolved plus SGS) over-predict the experimental data. This is consistent with previous results,[5] and it has been suggested that this variance might be decreased if a probe capable of higher resolution measurements is used in the experiments.

Finally, the radial distribution of the mean and RMS values of the mass fractions of several species are presented in Figures 6 - 13. The mean values of the mass fractions compare well with the experimental data. The RMS values do not agree with the data quite as well.

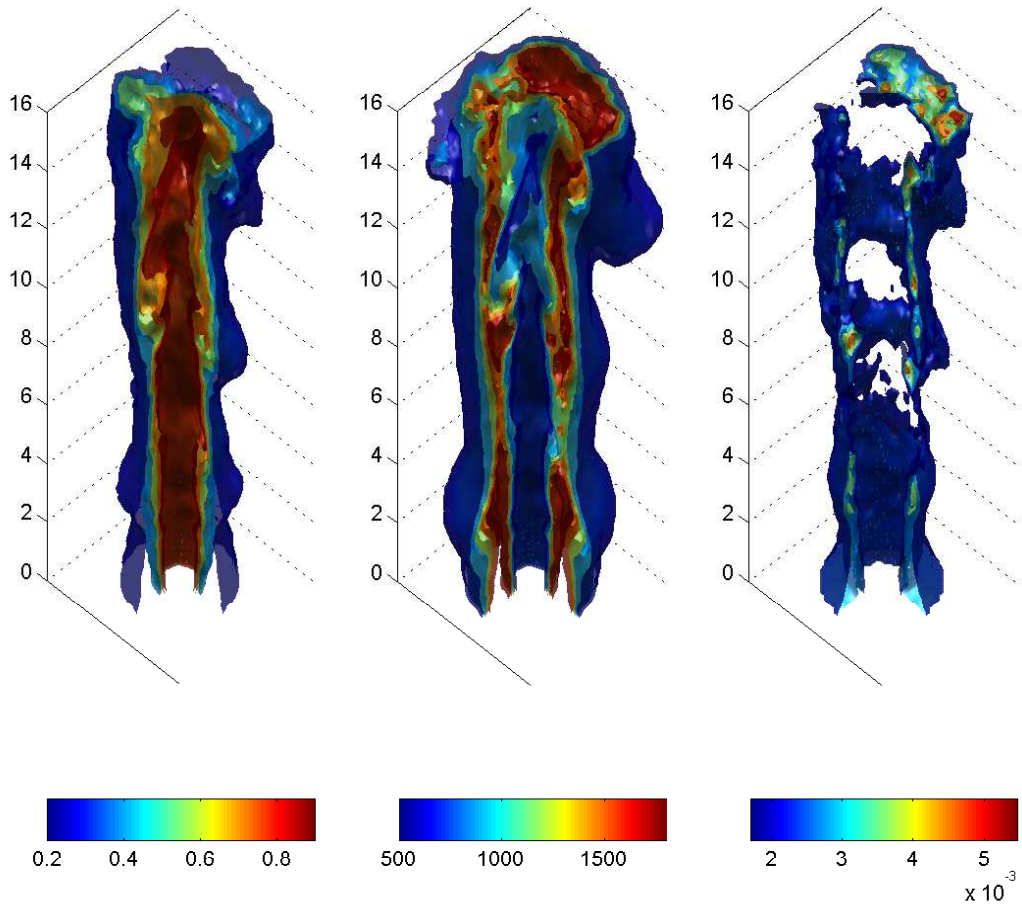

Figure 2: Instantaneous contours of the mixture fraction (left), temperature (center), and mass fraction of OH (right).

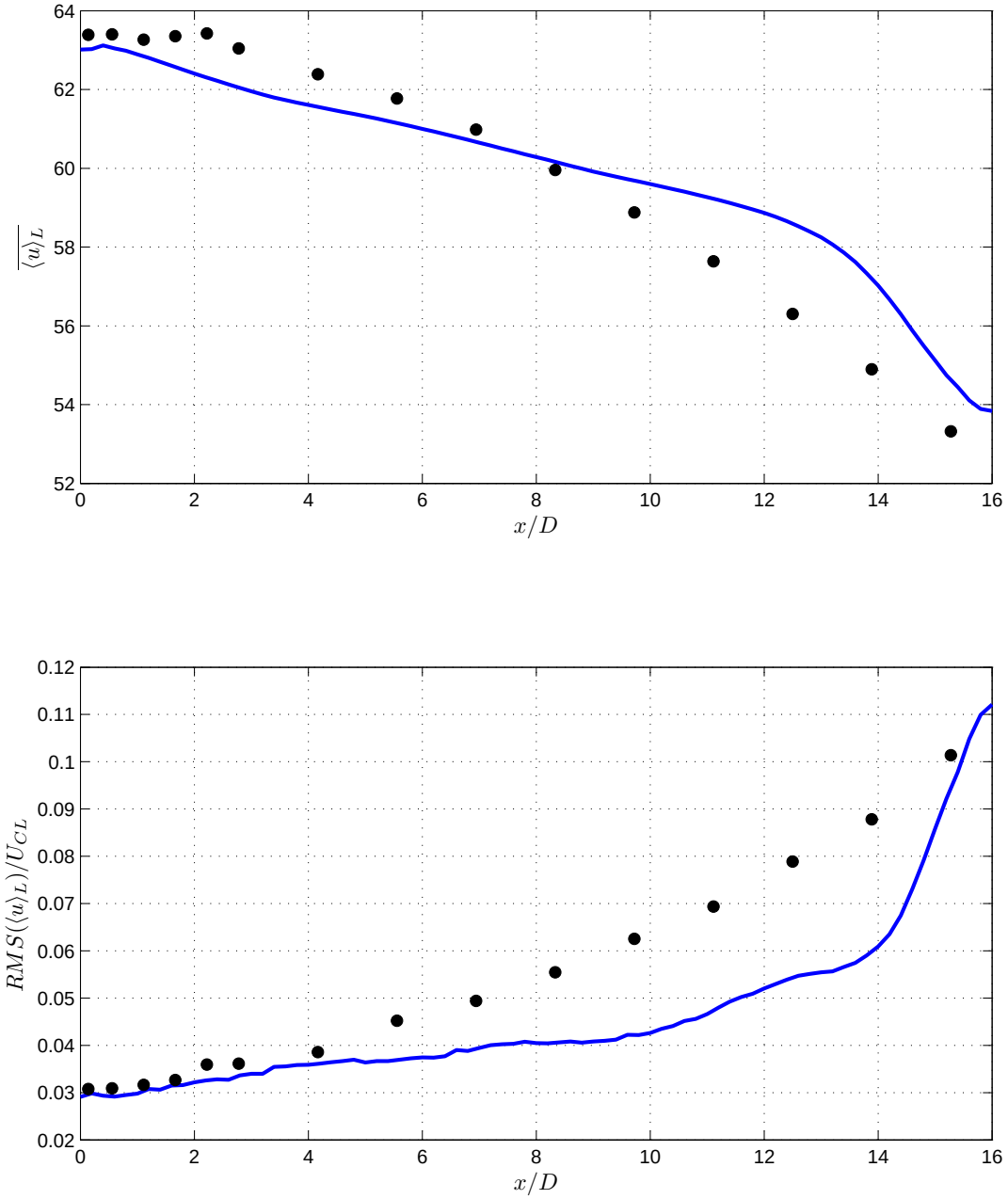

Figure 3: The mean and the RMS values of the axial velocity (m/s) at the centerline. U_{CL} denotes the mean axial velocity at the centerline. (•) experimental data.

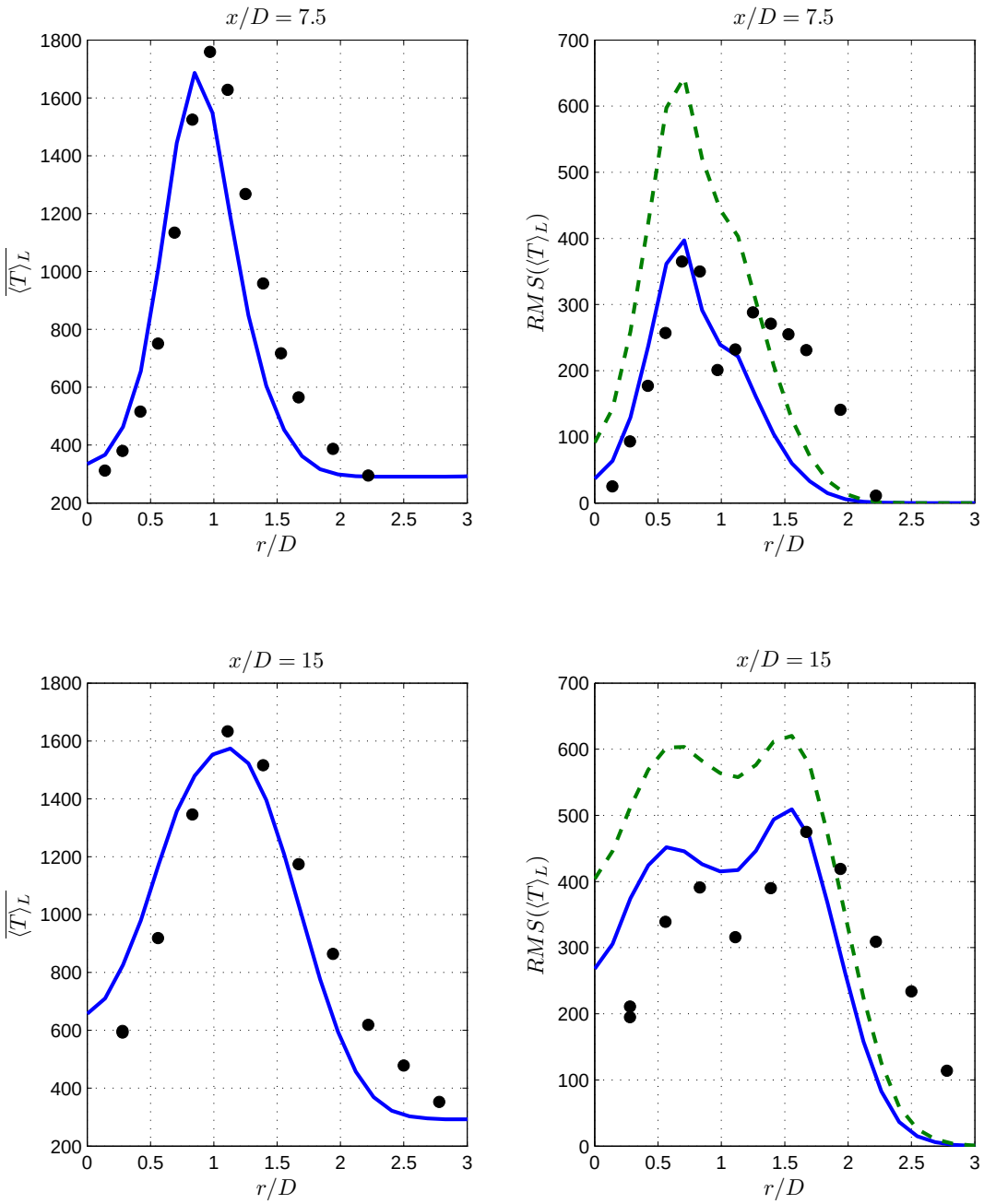

Figure 4: Radial distributions of the mean and the RMS values of the temperature at $x/D = 7.5,\ 15$. (•) experimental data, (——) resolved RMS value, (− −) total RMS value.

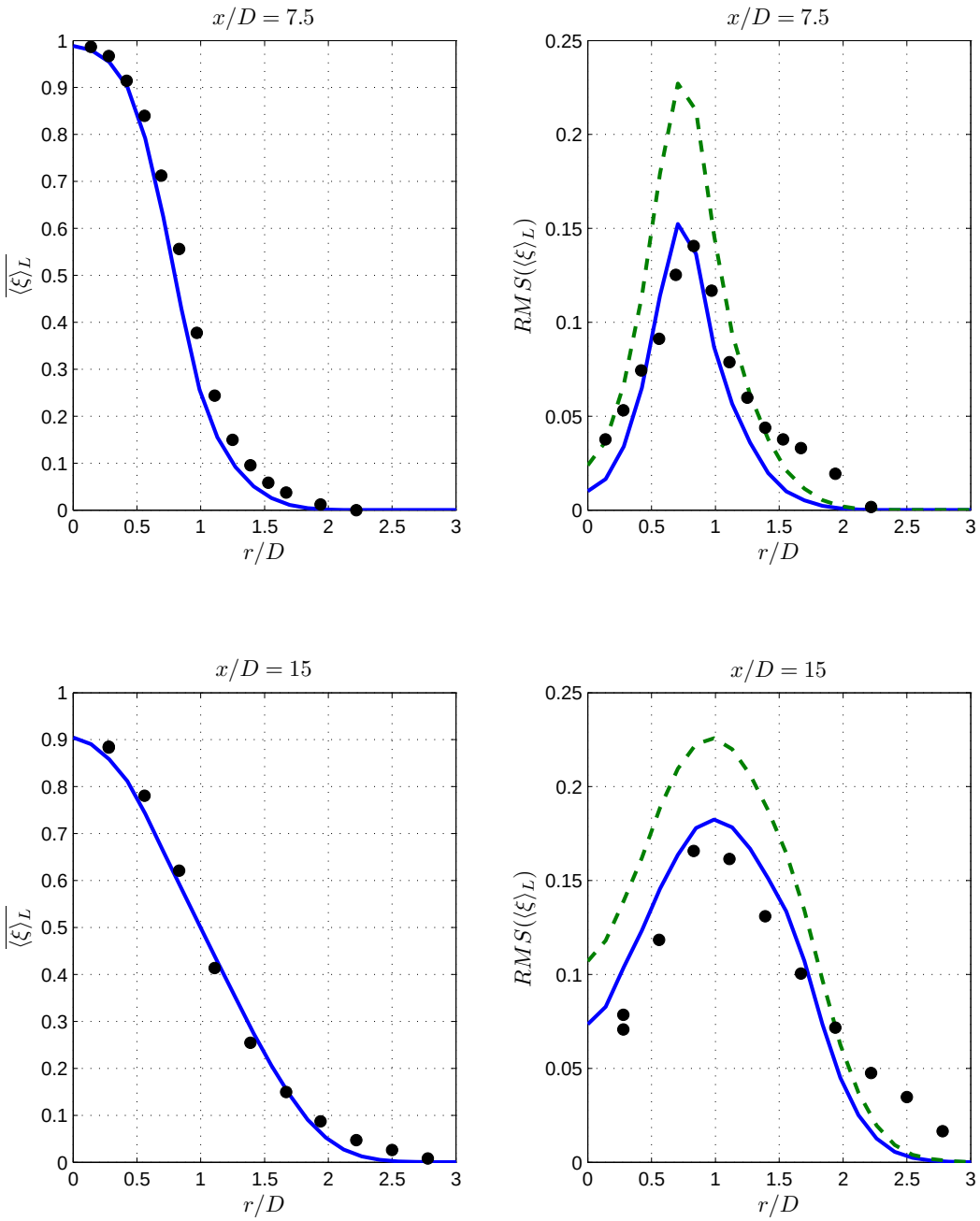

Figure 5: Radial distributions of the mean and the RMS values of the mixture fraction at $x/D = 7.5,\ 15$. (•) experimental data, (——) resolved RMS value, (− −) total RMS value.

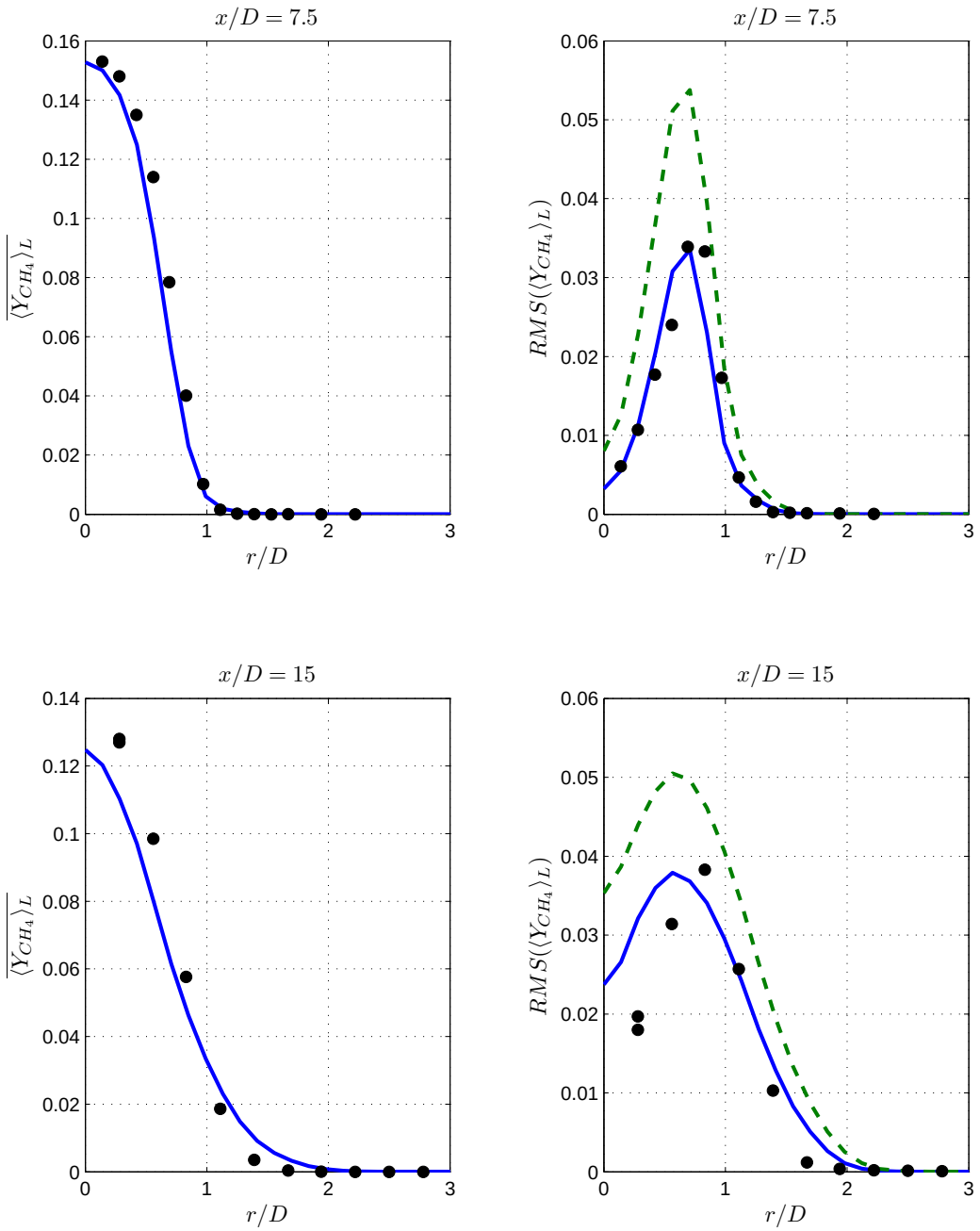

Figure 6: Radial distributions of the mean and the RMS values of the mass fraction of CH_4 at $x/D = 7.5,\ 15$. (•) experimental data, (——) resolved RMS value, (− −) total RMS value.

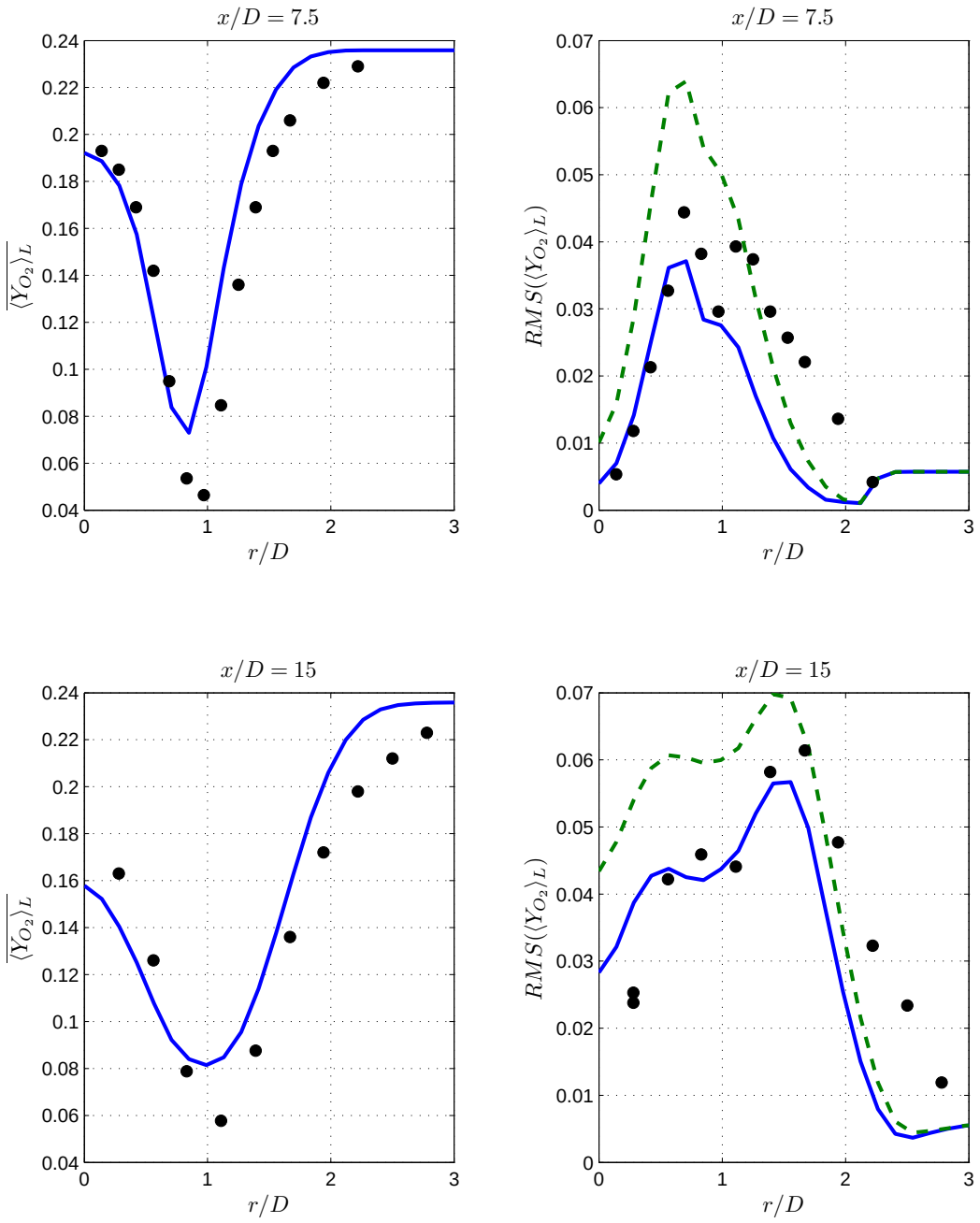

Figure 7: Radial distributions of the mean and the RMS values of the mass fraction of O_2 at $x/D = 7.5,\ 15$. (•) experimental data, (——) resolved RMS value, (− −) total RMS value.

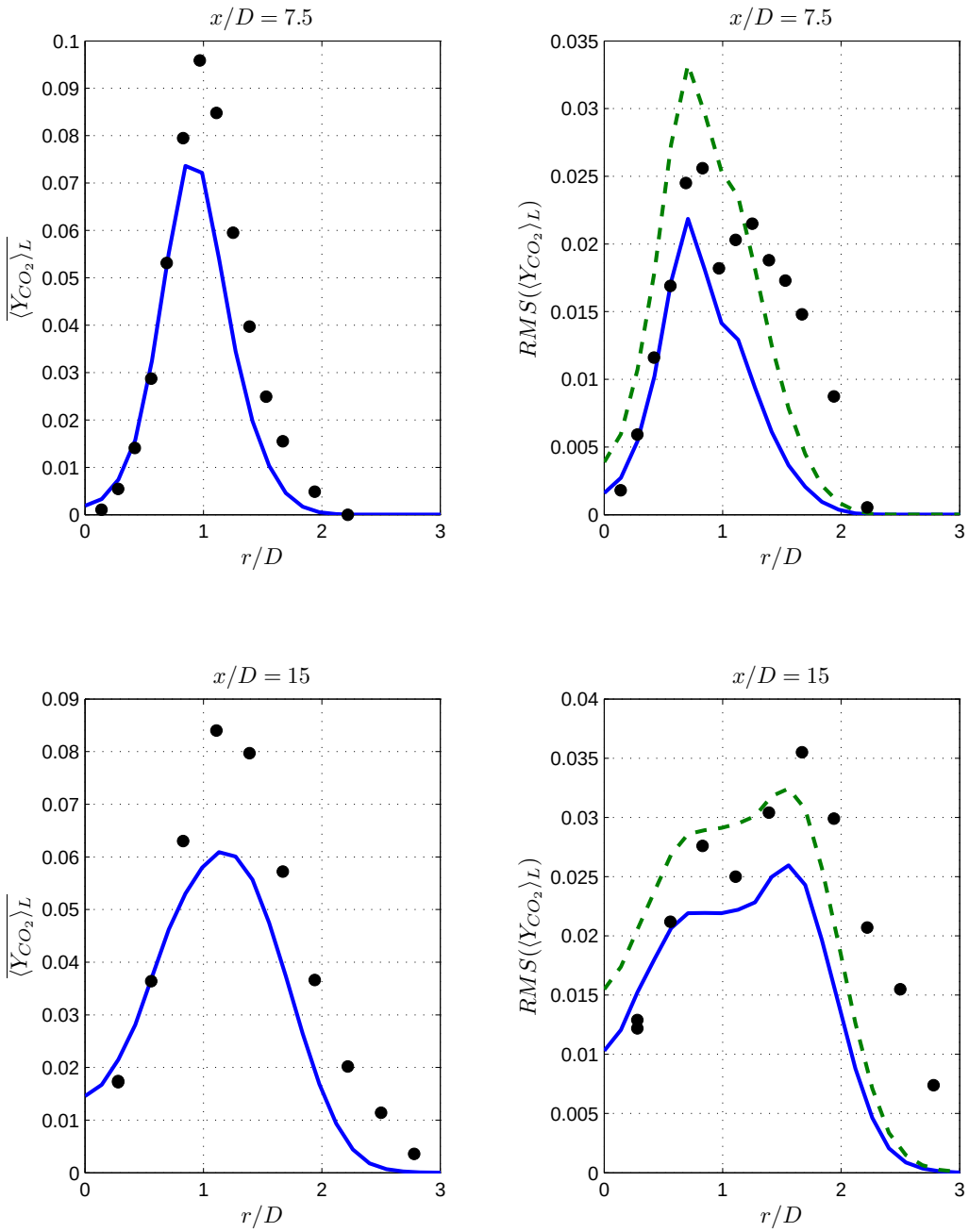

Figure 8: Radial distributions of the mean and the RMS values of the mass fraction of CO_2 at $x/D = 7.5,\ 15$. (•) experimental data, (——) resolved RMS value, ($- -$) total RMS value.

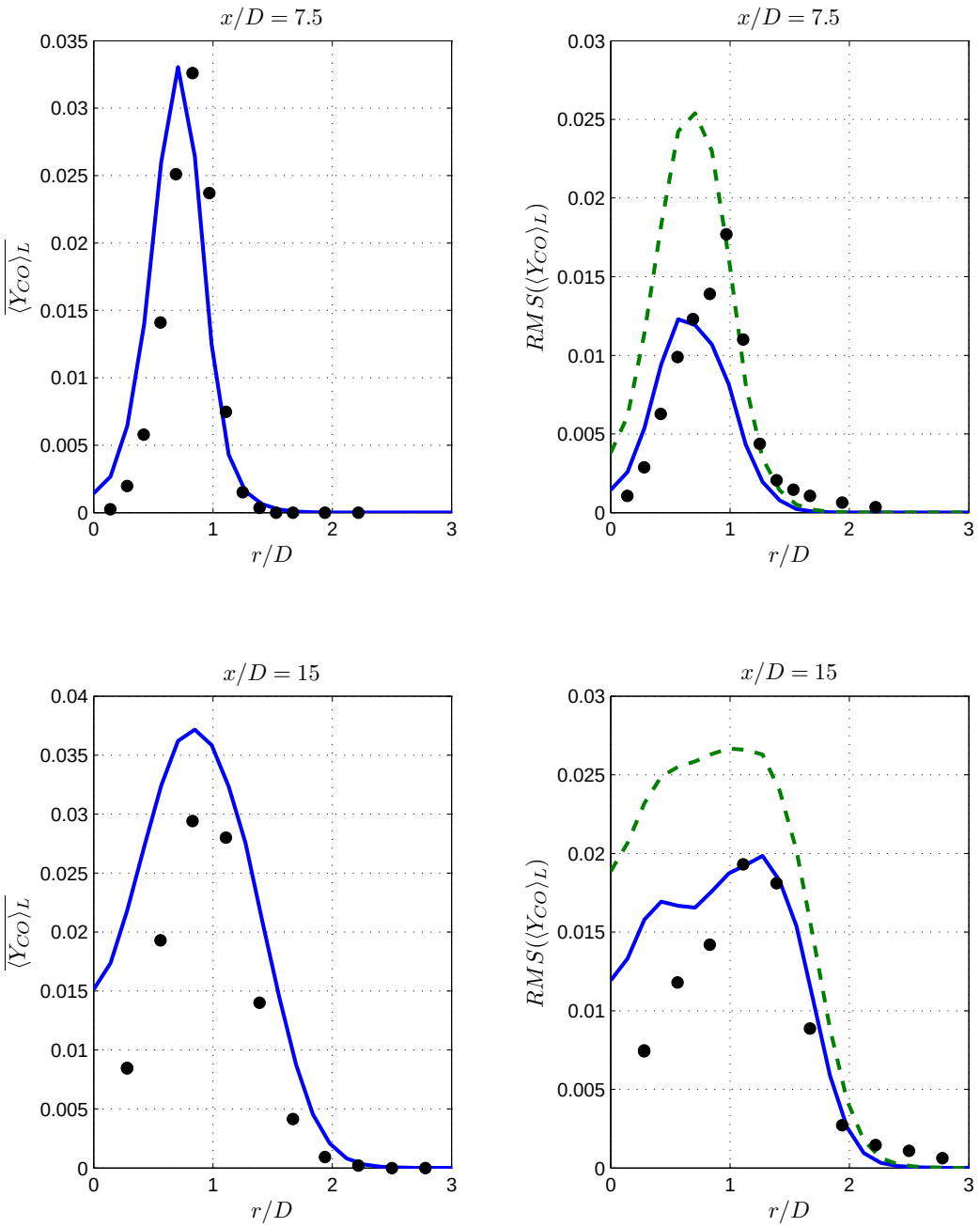

Figure 9: Radial distributions of the mean and the RMS values of the mass fraction of CO at $x/D = 7.5,\ 15$. (•) experimental data, (——) resolved RMS value, (− −) total RMS value.

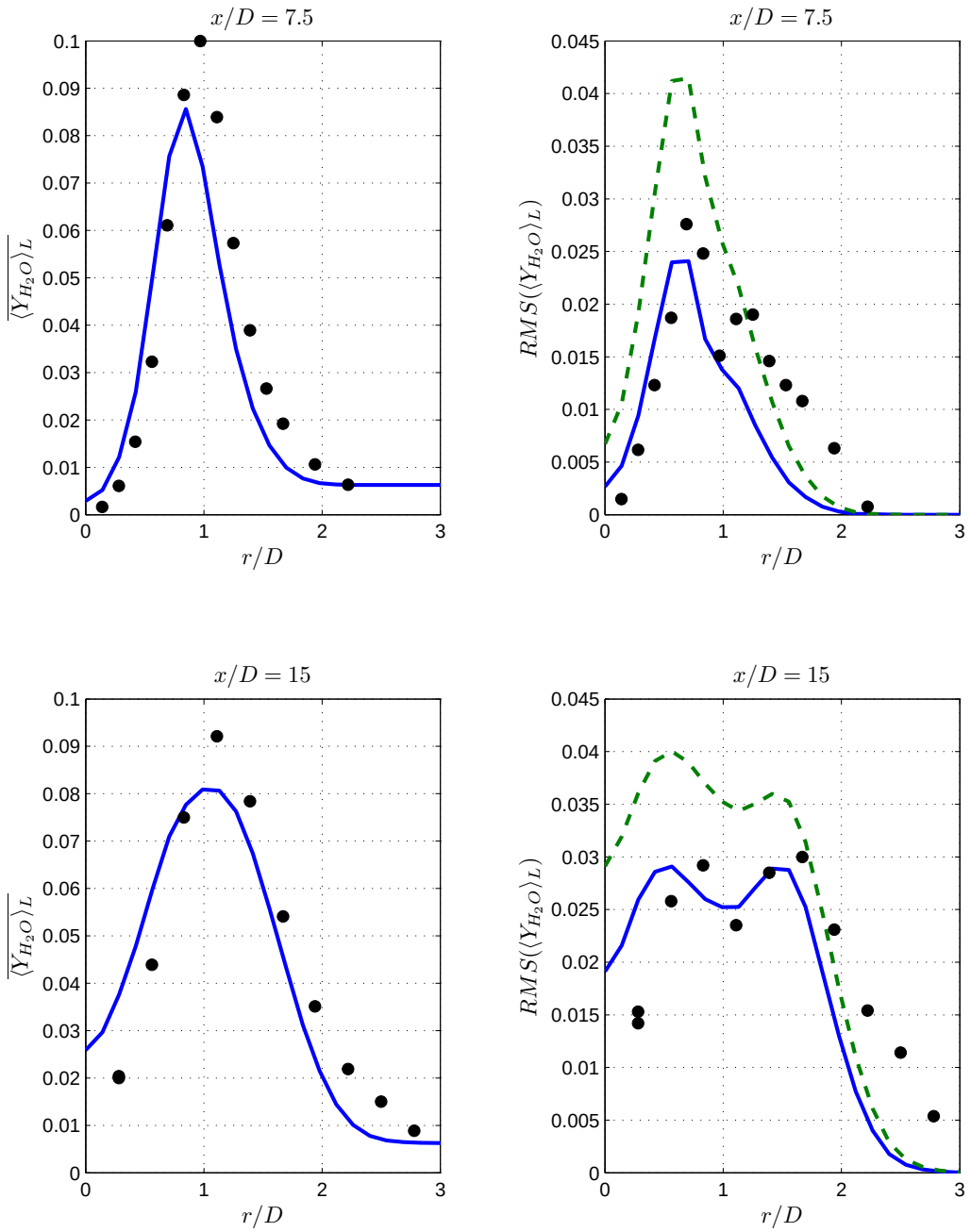

Figure 10: Radial distributions of the mean and the RMS values of the mass fraction of H_2O at $x/D = 7.5,\ 15$. (•) experimental data, (——) resolved RMS value, (− −) total RMS value.

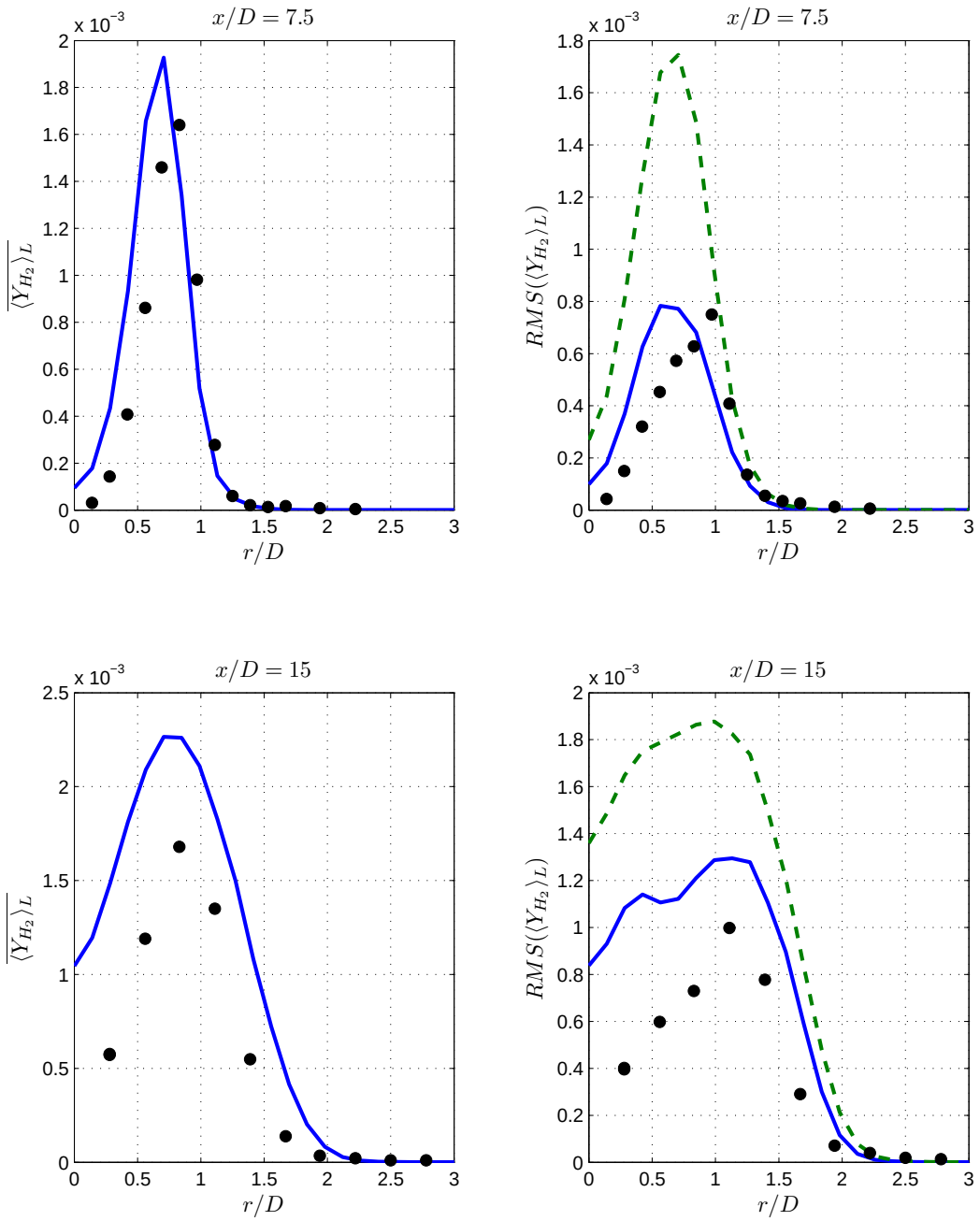

Figure 11: Radial distributions of the mean and the RMS values of the mass fraction of H_2 at $x/D = 7.5,\ 15$. (•) experimental data, (——) resolved RMS value, ($-\ -$) total RMS value.

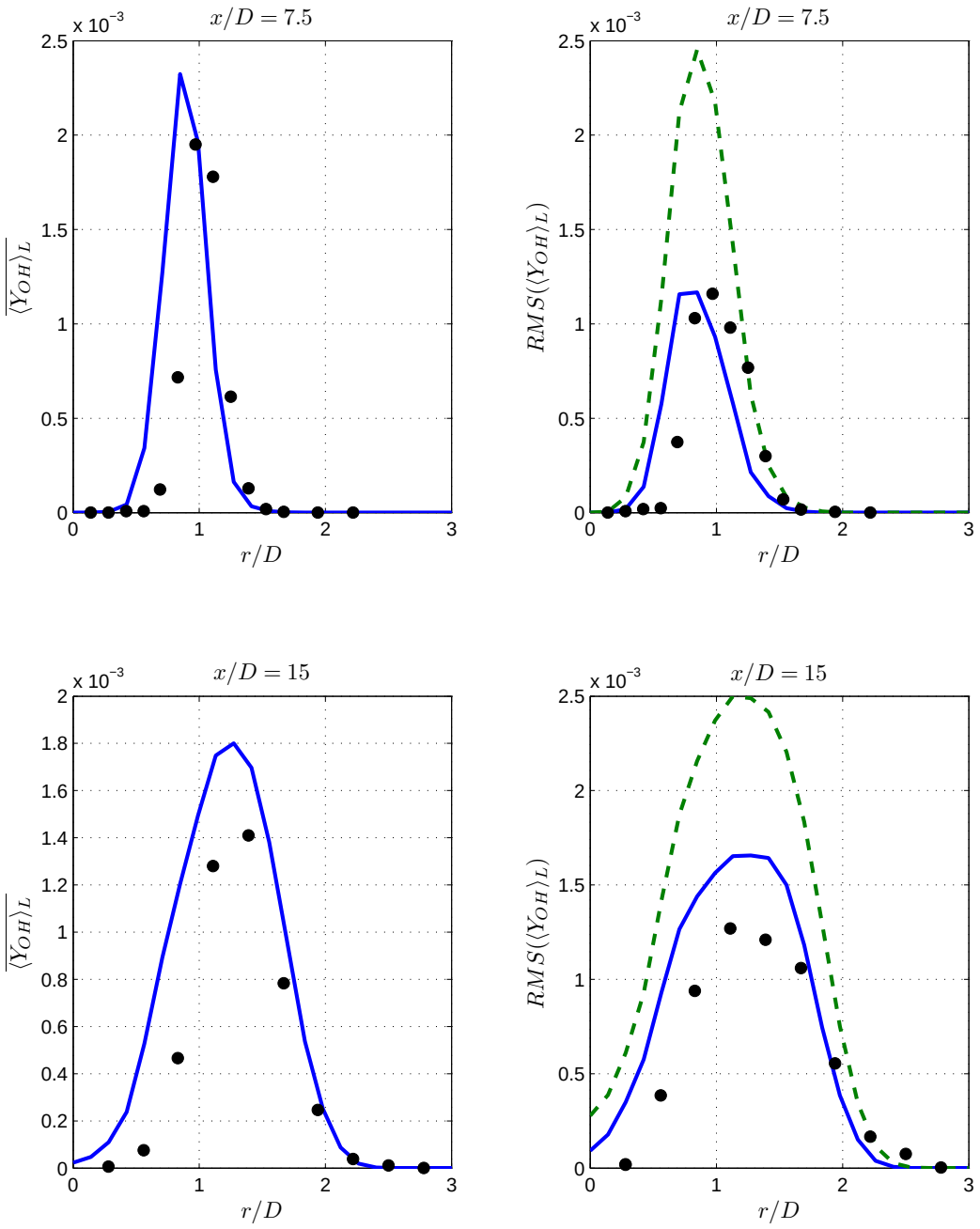

Figure 12: Radial distributions of the mean and the RMS values of the mass fraction of OH at $x/D = 7.5,\ 15$. (•) experimental data, (——) resolved RMS value, ($-\ -$) total RMS value.

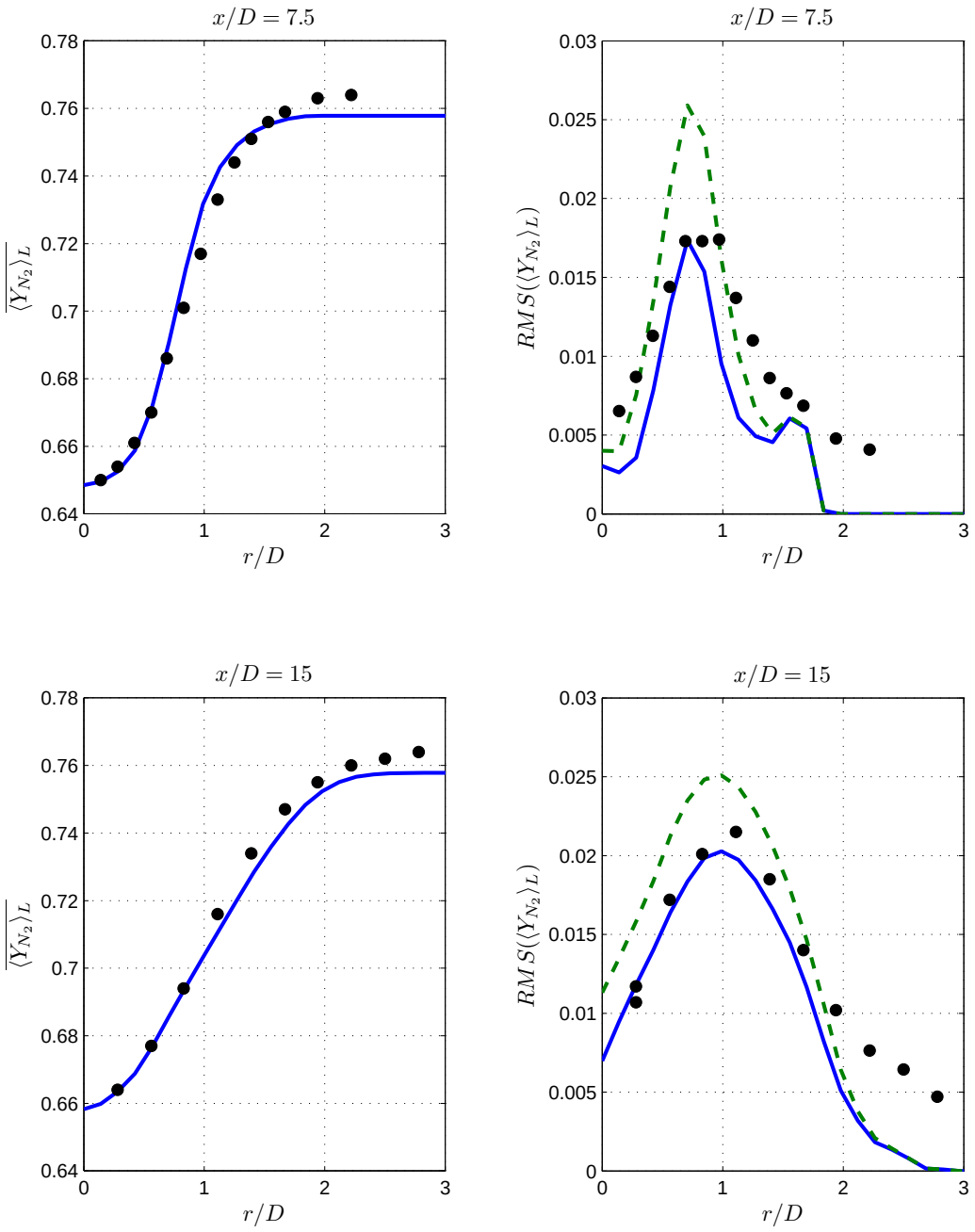

Figure 13: Radial distributions of the mean and the RMS values of the mass fraction of N_2 at $x/D = 7.5,\ 15$. (•) experimental data, (——) resolved RMS value, (− −) total RMS value.

4.0 CONCLUSIONS

Large eddy simulation is conducted of Sandia Flame D, which is a turbulent piloted non-premixed methane jet flame. The subgrid scale closure is based on the scalar filtered mass density function (SFMDF) methodology. The thermochemical variables are treated using a finite-rate chemistry model based on an augmented reduced mechanism. The modeled transport equation for the SFMDF of the thermochemical variables is solved by a hybrid finite-difference/Monte Carlo method.

The predictive capability of the method is assessed by comparisons with experimental data. In doing so, the ensemble (long time averaged) values of the thermochemical variables are considered. It is shown that the mean and the resolved RMS values are generally predicted well. However, the RMS quantities tend to over-predict the experimental data when the SGS contribution is taken into account.

This work shows that implementation of complex kinetics schemes in LES is now possible. The overall result is a scheme that is robust for treatment of turbulent reacting flows, and that is ready for the consideration of flames that exhibit extinction and re-ignition, such as Sandia Flames E and F.

BIBLIOGRAPHY

[1] Barlow, R. S. and Frank, J. H., Effects of Turbulence on Species Mass Fractions in Methane/Air Jet Flames, *Proc. Combust. Inst.*, **27**:1087–1095 (1998).

[2] Sandia National Laboratories, TNF Workshop website, Piloted Flames, http://www.ca.sandia.gov/TNF/pilotedjet.html, 2008.

[3] Jaberi, F. A., Colucci, P. J., James, S., Givi, P., and Pope, S. B., Filtered Mass Density Function for Large Eddy Simulation of Turbulent Reacting Flows, *J. Fluid Mech.*, **401**:85–121 (1999).

[4] Pope, S. B., *Turbulent Flows*, Cambridge University Press, Cambridge, UK, 2000.

[5] Sheikhi, M. R. H., Drozda, T. G., Givi, P., Jaberi, F. A., and Pope, S. B., Large Eddy Simulation of a Turbulent Nonpremixed Piloted Methane Jet Flame (Sandia Flame D), *Proc. Combust. Inst.*, **30**:549–556 (2005).

[6] Pitsch, H., Large-Eddy Simulation of Turbulent Combustion, *Annu. Rev. Fluid Mech.*, **38**:453–482 (2006).

[7] Givi, P., Sheikhi, M. R. H., Drozda, T. G., and Madnia, C. K., Large Scale Simulation of Turbulent Combustion, *Combust. Plasma Chem.*, **6**(1):1–9 (2008).

[8] Givi, P., Model Free Simulations of Turbulent Reactive Flows, *Prog. Energy Combust. Sci.*, **15**:1–107 (1989).

[9] Pope, S. B., Computations of Turbulent Combustion: Progress and Challenges, *Proc. Combust. Inst.*, **23**:591–612 (1990).

[10] Colucci, P. J., Jaberi, F. A., Givi, P., and Pope, S. B., Filtered Density Function for Large Eddy Simulation of Turbulent Reacting Flows, *Phys. Fluids*, **10**(2):499–515 (1998).

[11] Gicquel, L. Y. M., Givi, P., Jaberi, F. A., and Pope, S. B., Velocity Filtered Density Function for Large Eddy Simulation of Turbulent Flows, *Phys. Fluids*, **14**(3):1196–1213 (2002).

[12] Sheikhi, M. R. H., Drozda, T. G., Givi, P., and Pope, S. B., Velocity-Scalar Filtered Density Function for Large Eddy Simulation of Turbulent Flows, *Phys. Fluids*, **15**(8):2321–2337 (2003).

[13] Sheikhi, M. R. H., Givi, P., and Pope, S. B., Velocity-Scalar Filtered Mass Density Function for Large Eddy Simulation of Turbulent Reacting Flows, *Phys. Fluids*, **19**(9):095106 (2007).

[14] Nooren, P. A., Versiuis, M., Van der Meer, T. H., Barlow, R. S., and Frank, J. H., Raman-Rayleigh-LIF Measurements of Temperature and Species Concentrations in the Delft Piloted Turbulent Jet Diffusion Flame, *Appl. Phys. B*, **71**:95–111 (2000).

[15] Poinsot, T. and Veynante, D., *Theoretical and Numerical Combustion*, R. T. Edwards, Philadelphia, PA, 2nd edition, 2005.

[16] Sagaut, P., *Large Eddy Simulation for Incompressible Flows*, Springer Berlin Heidelberg, New York, NY, third edition, 2005.

[17] Aldama, A. A., Filtering Techniques for Turbulent Flow Simulations, *Lecture Notes in Engineering*, Vol. 49, Springer-Verlag, New York, NY, 1990.

[18] Vreman, B., Geurts, B., and Kuerten, H., Realizability Conditions for the Turbulent Stress Tensor in Large-Eddy Simulation, *J. Fluid Mech.*, **278**:351–362 (1994).

[19] Bardina, J., Ferziger, J. H., and Reynolds, W. C., Improved Turbulence Models Based on Large Eddy Simulations of Homogeneous, Incompressible, Turbulent Flows, Department of Mechanical Engineering Report TF-19, Stanford University, Stanford, CA, 1983.

[20] Eidson, T. M., Numerical Simulation of the Turbulent Rayleigh-Benard Problem using Subgrid Modelling, *J. Fluid Mech.*, **158**:245–268 (1985).

[21] O'Brien, E. E., The Probability Density Function (PDF) Approach to Reacting Turbulent Flows, in Libby, P. A. and Williams, F. A., editors, *Turbulent Reacting Flows*, *Topics in Applied Physics*, Vol. 44, Chapter 5, pp. 185–218, Springer-Verlag, Heidelberg, 1980.

[22] Borghi, R., Turbulent Combustion Modeling, *Prog. Energy Combust. Sci.*, **14**:245–292 (1988).

[23] Risken, H., *The Fokker-Planck Equation, Methods of Solution and Applications*, Springer-Verlag, New York, NY, 1989.

[24] Gardiner, C. W., *Handbook of Stochastic Methods for Physics, Chemistry and the Natural Sciences*, Springer-Verlag, New York, NY, 2nd edition, 1990.

[25] Karlin, S. and Taylor, H. M., *A Second Course in Stochastic Processes*, Academic Press, New York, NY, 1981.

[26] Pope, S. B., PDF methods for turbulent reactive flows, *Prog. Energy Combust. Sci.*, **11**:119–192 (1985).

[27] Pope, S. B., Lagrangian PDF Methods for Turbulent Flows, *Ann. Rev. Fluid Mech.*, **26**:23–63 (1994).

[28] Sung, C. J., Law, C. K., and Chen, J.-Y., An Augmented Reduced Mechanism For Methane Oxidation with Comprehensive Global Parametric Validation, *Proc. Combust. Inst.*, **27**:295–303 (1998).

[29] Xu, J. and Pope, S. B., PDF Calculations of Turbulent Nonpremixed Flames with Local Extinction, *Combust. Flame*, **123**:281–307 (2000).

[30] Pope, S. B., Computationally Efficient Implementation of Combustion Chemistry using *in situ* Adaptive Tabulation, *Combust. Theor. Model.*, **1**(1):41–63 (1997).

[31] Brown, P. N., Bryne, G. D., and Hindmarsh, A. C., VODE:A Variable-Coefficient ODE Solver, *SIAM J. Sci. Stat. Comput.*, **10**(5):1038–1051 (1989).

[32] Kee, R. J., Rupley, F. M., and Miller, J. A., Chemkin-III: A FORTRAN chemical kinetics package for the analysis of gas-phase chemical and plasma kinetics., Technical Report SAND96-8216, Sandia National Laboratories, Livermore, CA, 1996, Software available from Reaction Design Inc, www.reactiondesign.com.

[33] Givi, P. and Riley, J. J., Some Current Issues in the Analysis of Reacting Shear Layers: Computational Challenges, in Hussaini, M. Y., Kumar, A., and Voigt, R. G., editors, *Major Research Topics in Combustion*, pp. 588–650, Springer-Verlag, New York, NY, 1992.

[34] Drummond, J. P. and Givi, P., Suppression and Enhancement of Mixing in High-Speed Reacting Flow Fields, in Buckmaster, J. D., Jackson, T. L., and Kumar, A., editors, *Combustion in High-Speed Flows*, pp. 191–229, Kluwer Academic Publishers, The Netherlands, 1994.